Hollow core anti-resonant fiber with split cladding

Xiaosheng Huang,[1] Wenliang Qi,[1] Daryl Ho,[1] Ken-Tye Yong,[1] and Feng Luan,[2] Seongwoo Yoo[1]

[1]*The Photonics Institute, School of Electrical and Electronics Engineering, Nanyang Technological University, Singapore 639798, Singapore*
seon.yoo@ntu.edu.sg
[2]*College of Optoelectronics, Shenzhen University, Shenzhen 518060, China*
feng.luan@hotmail.com

Abstract: An improved design for hollow core anti-resonant fibers (HAFs) is presented. A split cladding structure is introduced to reduce the fabrication distortion within design tolerance. We use numerical simulations to compare the Kagome fibers (KFs) and the proposed split cladding fibers (SCFs) over two normalized transmission bands. It reveals that SCFs are able to maintain the desired round shape of silica cladding walls, hence improving the confinement loss (CL) compared to the KF and is comparable to that of the nested antiresonant nodeless fiber (NANF) with the same core size. In addition, the SCF allows stacking multiple layers of cladding rings to control the CL. The influences of the number of cladding layers and the cladding gap width on the CL of the SCFs have been studied. SCF with three cladding rings is fabricated by the stack-and-draw technique. A measured attenuation spectrum matches well with the calculation prediction. The measured near field mode patterns also prove the feasibility of our fiber design.

OCIS codes: (060.2280) Fiber design and fabrication; (060.2400) Fiber properties; (060.4005) Microstructured fibers.

References and links

1. T. A. Birks, P. J. Roberts, P. S. J. Russel, D. M. Atkin and T. J. Shepherd, "Full 2-D Photonic Bandgaps in Silica/Air Structures," Electron. Lett **31**(22), 1941-1943 (1995).
2. C. M. Smith, N.Venkataraman, M. T. Gallagher, D. Müller, J. A. West, N. F. Borrelli, D. C. Allan and K. W. Koch, "Low-loss hollow-core silica/air photonic bandgap fiber," Nature **424**, 657-659 (2003).
3. B. Beaudou, F. Gerôme, Y. Y. Wang, M. Alharbi, T. D. Bradley, G. Humbert, J.-L. Auguste, J.-M. Blondy, and F. Benabid, "Millijoule laser pulse delivery for spark ignition through kagome hollow-core fiber," Opt. Lett. **37**(9), 1430-1432 (2012).
4. M. G. Welch, K. Cook, R. A. Correa, F. Gerôme, W. J. Wadsworth, A. V. Gorbach, D. V. Skryabin, J. C. Knight, "Solitons in Hollow Core Photonic Crystal Fiber: Engineering Nonlinearity and Compressing Pulses," J. Lightwave Technol. **27**(11), 1644-1652 (2009).
5. Z. F. Wang, W. Belardi, F. Yu, W. J. Wadsworth, and J. C. Knight, "Efficient diode-pumped mid-infrared emission from acetylene-filled hollow-core fiber," Opt. Express **22**(18), 21872-21878 (2014).
6. A. M. Jones, A. V. Vasudevan Nampoothiri, A. Ratanavis, T. Fiedler, N. V. Wheeler, F. Couny, R. Kadel, F. Benabid, B. R. Washburn, K. L. Corwin, and W. Rudolph, "Mid-infrared gas filled photonic crystal fiber laser based on population inversion," Opt. Express **19**(3), 2309-2316 (2011).
7. P. Roberts, F. Couny, H. Sabert, B. J. Mangan, D. P. Williams, L. Farr, M. W. Mason and A. Tomlinson, "Ultimate low loss of hollow-core photonic crystal fibers," Opt. Express **13**(1), 236-244 (2005).
8. F. Benabid, P. Roberts, F. Couny and P. S. Light, "Light and gas confinement in hollow-core photonic crystal fiber based photonic microcells," J. European Opt. Soc **4**, 09004 (2009). https://www.jeos.org/index.php/jeos_rp/article/view/09004
9. F. Couny, F. Benabid, P. J. Roberts, P. S. Light and M. G. Raymer, "Generation and photonic guidance of multi-octave optical-frequency combs," Science **318**(5853), 1118-1121 (2007).
10. F. Poletti, "Nested antiresonant nodeless hollow core fiber," Opt. Express **22**(20), 23807-23828 (2014).

11. L. Vincetti and V. Setti, "Confinement loss in kagome and tube lattice fibers: comparison and analysis," J. Lightwave Technol. **30**(10), 1470-1474 (2012).
12. A. N. Kolyadin, A. F. Kosolapov, A. D. Pryamikov, A. S, Biriukov, V. G. Plotnichenko and E. M. Dianov, "Light transmission in negative curvature hollow core fiber in extremely high material loss region," Opt. Express **21**(8), 9514-9519 (2013).
13. F. Yu, W. J. Wadsworth and J. C. Knight, "Low loss silica hollow core fibers for 3–4 μm spectral region," Opt. Express **20**(10), 11153-11158 (2012).
14. F. Benabid, J. C. Knight, G. Antonopoulos and P. S. J. Russell, "Stimulated Raman scattering in hydrogen-filled hollow-core photonic crystal fiber," Science **298**(5592), 399-402 (2002).
15. G. J. Pearce, G. S. Wiederhecker, C. G. Poulton, S. Burger and J. R. P. St, "Models for guidance in kagome-structured hollow-core photonic crystal fibers," Opt. Express **15**(20), 12680-12685 (2007).
16. M. Alharbi, T. Bradley, B. Debord, C. Fourcade-Dutin, D. Ghosh, L. Vincetti, F. Gérôme and F. Benabid, "Hypocycloid-shaped hollow-core photonic crystal fiber Part II: Cladding effect on confinement and bend loss," Opt. Express **21**(23), 28609-28616 (2013).
17. B. Debord, M. Alharbi, T. Bradley, C. Fourcade-Dutin, Y. Y. Wang, L. Vincetti, F. Gérôme and F. Benabid, "Hypocycloid-shaped hollow-core photonic crystal fiber Part I: Arc curvature effect on confinement loss," Opt. Express **21**(23), 28597-28608 (2013).
18. Y. Y. Wang, N. V. Wheeler, F. Couny, P. J. Roberts and F. Benabid, "Low loss broadband transmission in hypocycloid-core Kagome hollow-core photonic crystal fiber," Optics letters **36**(5), 669-671 (2011).
19. S. Février, B. Beaudou and P. Viale, "Understanding origin of loss in large pitch hollow-core photonic crystal fibers and their design simplification," Opt. Express **18**(5), 5142-5150 (2010).
20. A. D. Pryamikov, A. S. Biriukov, A. F. Kosolapov, V. G. Plotnichenko, S. L. Semjonov and E. M. Dianov, "Demonstration of a waveguide regime for a silica hollow-core microstructured optical fiber with a negative curvature of the core boundary in the spectral region> 3.5 μm," Opt. Express **19**(2), 1441-1448 (2011).
21. F. Couny, F. Benabid and P. S. Light, "Large Pitch Kagome-Structured Hollow-Core PCF," in *Conference on Lasers and Electro-Optics*, OSA Technical Digest Series (CD) (Optical Society of America, 2007), paper CWF1. https://www.osapublishing.org/abstract.cfm?uri=CLEO-2007-CWF1
22. L. Vincetti and V. Setti, "Extra loss due to Fano resonances in inhibited coupling fibers based on a lattice of tubes," Opt. Express **20**(13), 14350-14361 (2012).
23. S. G. Leon-Saval, A. Argyros and J. Bland-Hawthorn, "Photonic lanterns: a study of light propagation in multimode to single-mode converters," Opt. Express **18**(8), 8430-8439 (2010).
24. W. Belardi and J. C. Knight, "Hollow antiresonant fibers with reduced attenuation," Opt. Lett. **39**(7), 1853-1856 (2014).
25. F. Couny, F. Benabid and P. Light, "Large-pitch kagome-structured hollow-core photonic crystal fiber," Opt. Lett. **31**(24), 3574-3576 (2006).
26. L. Vincetti and V. Setti, "Waveguiding mechanism in tube lattice fibers," Opt. Express **18**(22), 23133-23146 (2010).
27. W. Belardi and J. C. Knight, "Effect of core boundary curvature on the confinement losses of hollow antiresonant fibers," Opt. Express **21**(19), 21912-21917 (2013).
28. F. Benabid, "Hollow-core photonic bandgap fiber: new light guidance for new science and technology," Philos Trans A Math Phys Eng Sci **364**(1849), 3439-3462 (2006).

1. Introduction

Since the first theoretical demonstration in 1995 [1], hollow core photonic crystal fibers (HC-PCFs), as a remarkable breakthrough in fiber optics, make it possible to guide light in the air core. This unique guiding property promises the potentials of achieving lower Rayleigh scattering, higher damage threshold and lower nonlinearity compared to conventional fibers [2]. Hence, HC-PCFs have promising application in areas such as high power delivery [3], pulse compression [4], and gas laser systems [5,6].One type of HC-PCFs is hollow core photonics bandgap fibers (HC-PBGFs) whose record loss is 1.2 dB/km at 1.62 μm [7]. However, this HC-PBGF typically has a relatively narrow transmission band [8]. The other type of HC-PCF, is so-called hollow core antiresonant fibers (HAFs), whose guiding property relies on the combination of anti-resonance and inhibited coupling to low density of states cladding modes [9,10]. The HAF has received ever-increasing interest for its unique transmission property. It permits relatively low transmission loss, and multiple broad transmission bands [11]. Furthermore, because its transmission loss is largely determined by

the scattering from the cladding layers rather than the material loss, the HAF is able to transmit the mid-IR range [12]. Demonstration of 3.05 μm transmission was reported with a background loss of 34 dB/km [13].

The HAF was first demonstrated in the Kagome structure [14]. Investigation to reduce the confinement loss (CL) has been the main focus of the fiber design. The influence of the number of the cladding ring layers is found insignificant to suppress the CL after two cladding layers [15,16]. On the other hand, the hypocycloid-core shape was reported to enhance the coupling inhibition between the core and cladding modes. It offers measured attenuation with a lowest loss 17 dB/km at around 1 um spectral range by optimizing the core contour [17]. Thus, it appears that core shaping would play a more crucial role in the CL reduction as long as the cladding is made up of 2 layers or more [18]. This observation leads us to exploring a design to maintain the cladding inner wall shape that forms the air core. For example, the KF typically suffers from distorted core shaped caused by the fiber drawing process. Such deformation can be avoided by introducing radial gaps in the cladding area.

In this work we present an alternative design for the KFs to reduce the CL. The cladding layers are radially split in our design to alleviate the core shape deformation during the fiber drawing process. The gaps created by the radial separation do not deteriorate the fiber performance, and the CL comparable to the KFs is attainable in the split cladding design. Furthermore, the proposed design helps to diminish vertices formed in the cladding layers during the fiber fabrication, which is additional benefit toward low transmission loss. Although there are several simplification designs of HAF with single cladding ring layer [13,19,20], their cladding is not scalable with additional layers [12,13]. Our split cladding structure allows multiple cladding layers to control the CL, which is useful for many applications including a gas-filled Raman scattering. The details of our theoretical investigation and fiber fabrication are represented as below.

2. Split cladding fiber design

The tube lattice fiber (as shown in the TLF structure in Fig. 1) has a circular air core formed by surrounding silica walls in the cladding. This ideal fiber shape is altered by the high temperature fiber drawing process due to the surface tension of molten silica. The high temperature fiber drawing introduces deformation in the core shape from circular to hexagon-like core. The resulted structure is illustrated in Fig. 1 as KF. The core-cladding boundary of the KF consists of two different walls denoted as 1 and 2. This alternating boundaries account for the core shape deformation [21]. In addition to the core deformation, the fabrication process produces vertices in the cladding layers. The induced vertices cause extra loss due to Fano resonances between core modes and cladding modes [22], and limit the performance of KFs. To avoid the fabrication deformation and reduce the number of high resonant vertices, we propose a modified design composed of split claddings.

2.1 Design

The proposed split cladding fiber (SCF) is represented in the Fig. 1. An ideal structure neglecting the fabrication deformation is represented as ISC in Fig. 1. The structure including the fabrication deformation is denoted as SCF in Fig. 1. As shown in the figure, the number of cladding vertices in SCF is much less than that in KF, and the silica walls in SCF are more rounded as compared to the KF. Moreover, the SCF structure possesses only one wall boundary shape, diminishing core shape distortion without compromising the desired negative curvature. It may be of concern that the discontinuous cladding layer would induce additional loss. Thus we investigate the loss in the SCF in a broad transmission band. A two cladding layer SCF is assumed in the theoretical study.

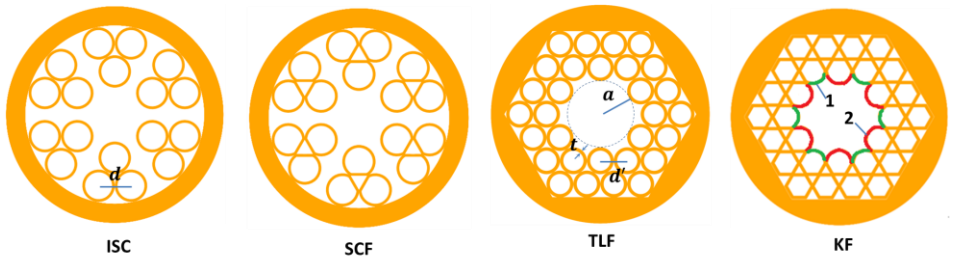

Fig. 1. Fiber fabrication induced distortion in KF and proposed SCF structures. The surface tension of molten silica during the fiber drawing modifies the structures deviated from the ideal cases. TLF represents the ideal structure of the kagome fiber (KF). ISC represents the ideal structure of the split-cladding fiber (SCF) *a*, *d*, and *t* denote inner core radius, pitch size and core wall thickness respectively. The different wall shapes in the KF are indicated by 1 and 2.

We used the open source finite-element software Polymode [23] to perform our numerical simulations. Figure 2 shows the calculated transmission spectra of the different fiber structures. All the fibers have the same inner core radius (a = 9.76 μm) and silica wall thickness (t = 1 μm). The pitch size, *d'*, in the TLF and KF is 8 μm while the SCF and ISC has 11.8 μm of the pitch size, *d*. Normalized frequency, *F*, is defined as $F = (2tf/c) \times \sqrt{n^2 - 1}$, with f being the frequency, n the dielectric refractive index (here, n = 1.45), and c the vacuum light speed. The local peak losses observed in the transmission bands in Fig. 2(a) are caused by coupling between the cladding mode and the fundamental mode [24]. The results show that the ISC can mark the same CL as the TLF. More interestingly, the ISC supports a broader transmission band. When considering the effect of the surface tension caused by the drawing process, the KF and SCF will represent more realistic structures. It is clear from Fig. 2 that the SCF promises the same performance as the ISC with no increase in the CL. The structure deformation occurred in the SCF is moderate, and keeps most of the silica walls rounded, creating only small number of high resonant vertices. However, the transition from the TLF to the KF is accompanied with transforming most of the cladding walls to flat surfaces, hence large number of vertices. The vertices enhance Fano resonances between core and cladding modes and increase the transmission loss [22].

As shown in Fig. 2, the CL is one magnitude lower in the SCF than in the KF and is comparable to that in the nested antiresonant nodeless fiber (NANF) with the same core size [10]. We note that the CL becomes lower in NANF than 2SCF when the transmission window moves towards longer wavelength region (F < 1). However, modified 2SCF can reach to similar CL as NANF in the longer wavelength region. We discuss about the long wavelength region in Section 2.2. We also note that the SCF exhibits as broad transmission window as the ISC. The pitch size in SCF, *d'*, is larger than its counterpart in the KF (or the TLF), *d*, when the same core size is compared. The larger pitch size accounts for the broader transmission bands when core wall thickness is fixed [25]. Besides, in the fiber fabrication, the KF fiber drawing requires precise pressure control to maintain the negative curvature of the core-cladding boundary. This is not necessary in the SCF fiber fabrication.

The insignificance of the structural deformation is confirmed again in the effective refractive index overlap between the SCF and the ISC as represented in Fig. 2(b).

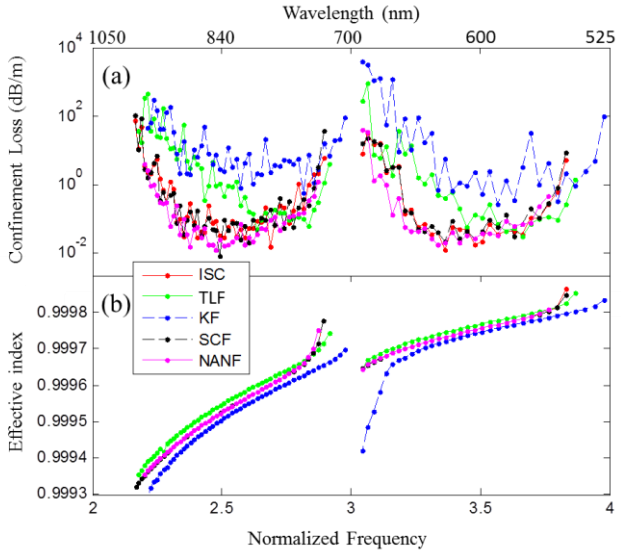

Fig. 2. (a) Confinement loss and (b) effective refractive index with normalized frequency in different anti-resonant fiber structures: tube lattice fiber (TLF, green curve), kagome fiber (KF, blue curve), split cladding hollow core fiber (SCF, black curve), ideal split-cladding fiber (ISC, red curve) and nested antiresonant nodeless fiber (NANF, purple curve). All the fibers have the same inner core radius.

2.2 Effect of second cladding ring layer on the transmission loss

We further investigate the effect of the cladding layers on the CL in the SCF. Because there is no significant gain on confinement loss from increasing the cladding layer more than two layers [15,16], the SCF with one and two layers are studied. Figure 3 compares the confinement loss between 1-ring SCF (1SCF, red line, similar to the structure proposed in [12]) and 2-ring SCF (2SCF, blue line) over four transmission bands. The CL of 2SCF is almost one magnitude lower than 1SCF at the first transmission band, $0.5 < F < 1$. The difference in the CL between the 1SCF and the 2SCF gets smaller when the transmission band moves to larger F. Eventually, the 2SCF does not help to reduce the CL at the fourth transmission band, $3 < F < 4$. The observation suggests that the second ring is more important at lower frequency regions (or longer wavelength regions). The longer wavelength propagates at a larger propagation angle, and hence more vulnerable to leaking. An extra layer can help to avoid the energy leakage via reflection, and this effect becomes more noticeable at longer wavelength regions. The localised sharp peaks in Fig. 3 are caused by coupling between silica cladding mode and the fundamental mode [24]. The faster oscillation in the transmission spectrum of the 2SCF indicates more silica cladding modes as compared to the 1SCF. We note that the SCF with three layers does not provide better performance than the two layers SCF.

The silica wall thickness of the second ring, t_2, can also influence the loss performance of the fiber. By selecting an appropriate t_2, the confinement loss at a certain transmission band can be greatly reduced. For example, the CL of 2SCF at the 4th transmission band is improved by one magnitude order when $t_2 = 0.5t$ (black dotted line). The CL of 2SCF at the 3rd transmission band also improves with $t_2 = 1.08t$ (purple dotted line). The mechanism of the CL reduction by adjusting t_2 is not clear at the moment. We only speculate that the different ring thicknesses would inhibit coupling of "dielectric" modes [26] between different ring sizes. This may propose an alternative route to reduce the CL in the antiresonant fibers. However, it should be carefully examined in future including experimental confirmation.

In Fig. 4, the CL of NANF and 2SCF in long wavelength region (F < 1) is compared. We already showed that the 2SCF performs as good as NANF in the short wavelength region (F > 2) in Fig. 2. To verify the accuracy of our simulation, we used the same fiber parameters reported in [10] (See the orange curve in Fig. 6 in [10]) to draw the red curve in Fig. 4. As clearly shown, our results match well with the reported CL in [10], which validates our simulation results. The CL of 2SCF is then calculated and compared to NANF in Fig. 4. We see that the 2SCF possesses higher CL than NANF. However, this can be improved. By differentiating the capillary size of the second ring from the first ring, we can modify the 2SCF design as shown in the inset in Fig. 4. This modified 2SCF reaches to the CL of NANF.

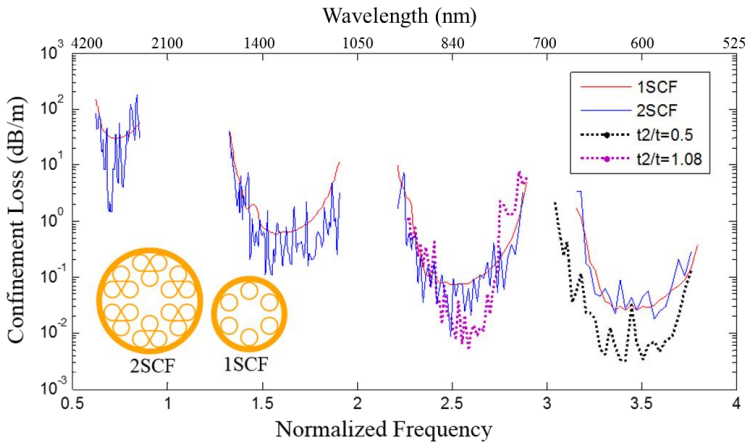

Fig. 3. Comparison of confinement loss among different SCF structures: 1-ring split cladding hollow core fiber (1SCF, red solid line), 2-ring split cladding hollow core fiber (2SCF, blue dash line), 2SCF with second ring wall thickness $t_2 = 0.5t$ (black dotted line) and 2SCF with $t_2 = 1.08t$ (purple dotted line). All these structures have the same inner core radius a = 9.76 μm, pitch size d = 11.8 μm and core wall thickness t = 1 μm.

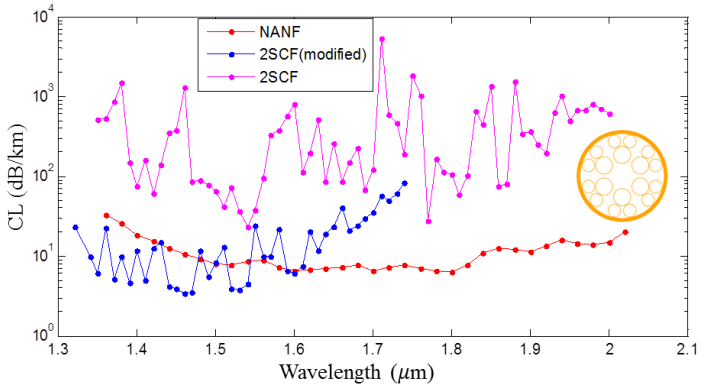

Fig. 4. Comparison of confinement loss between NANF and SCF in first resonant band (F < 1): NANF with the same geometry as in [10] (red line), 2SCF (magenta line), 2SCF with d_2/d = 0.77 (blue line). All these structures have the same inner core radius a = 13 µm, d = 18.72 µm and t = 0.55 μm. Inset shows the structure of 2SCF with smaller capillaries in second ring.

2.3 Effect of normalized gap width on the transmission loss

In Fig. 5, the CL at normalized frequencies of F=2.63 (blue line) and effective area of fundamental mode (green line) are evaluated for different values of the normalized gap width,

$g = w/a$, where w is the actual gap width, and a is the inner core radius. As a maintains the same, structure with larger gap width has smaller pitch size. The lowest basement loss is attainable in $g = 0.3 \sim 0.4$. In the region of $g < 0.3$, the cladding hole size becomes close to the hollow core size, which makes the effective mode index of the cladding air mode close to the fundamental mode effective index. This favours the coupling between the fundamental mode and the cladding mode, which limits the CL. Figure 6 supports occurrence of such coupling. The effective indices of fundamental mode (mode A) at different gap widths remain same because of the same inner core radius. In contrast, the cladding airy mode (mode B) effective index gets closer to the index of the mode A when the structure contains a narrower g.

Besides, when the gap width becomes wider, $g > 0.5$, the CL becomes higher. The fast increasing of effective mode area at this range accounts for the increased CL. The observation in Fig. 5 is applicable to other normalized frequencies, F, albeit varied in CL values.

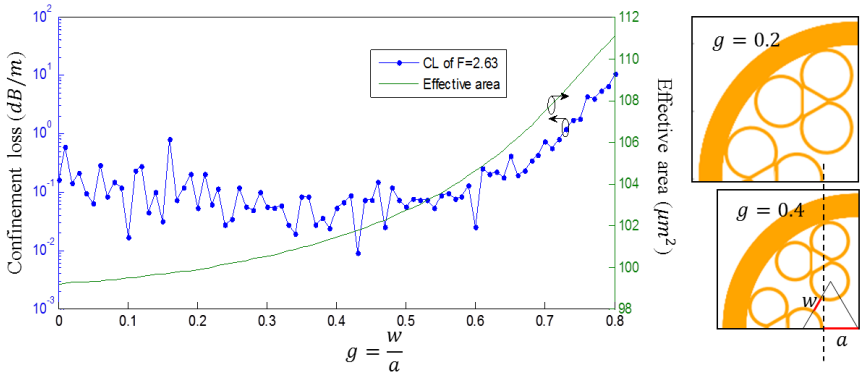

Fig. 5. Confinement loss (blue line) and effective area (green line) of F=2.63 vs. the normalized gap width, = w/a, where w is the gap width, a is the inner core radius. The a is assumed as 9.76 μm.

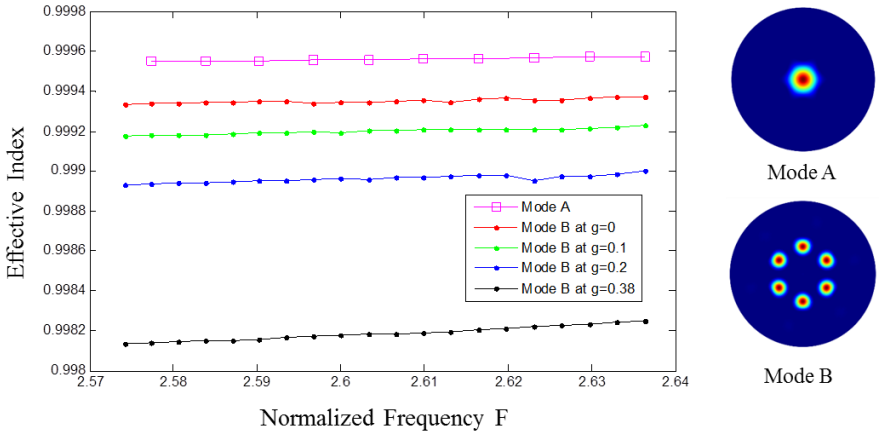

Fig. 6. The effective refractive indices of the fundamental mode (mode A) and cladding airy mode (mode B) at different gap widths. The mode A plots the same curve regardless of the gap width because the inner core radius is fixed.

To investigate the origin of the localised sharp peaks observed in Fig. 5, we analyze effective index at a specific g of 0.16 where one of the sharp peaks appears. Figure 7 shows the evolution of the effective index with varied g for mode A (green line) and B (red line). As expected, the peak of confinement loss (blue dashed line) corresponds to the crossing point of effective indices of modes A and B. Hence, we conclude that the local loss peak is indeed

caused by the strong coupling between modes A and B. It should be noted that the same coupling is observed for other loss peaks in Fig. 5, which leads us to generalize this explanation to all loss peaks. Our conclusion is in agreement with [27].

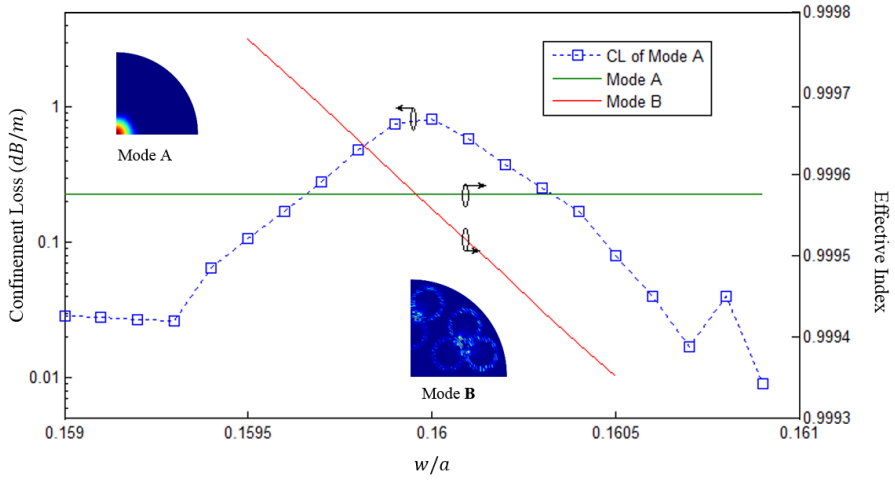

Fig. 7. The fundamental mode (green – mode A) and a cladding mode (red – mode B) vs. the normalised gap width, *g*. The confinement loss (shown in blue dash line) peaks where effective index of mode A and mode B are matched.

3. Fiber fabrication and experimental results

We used the conventional stack-and-draw technique [28] to fabricate the SCF with three cladding rings. The scanning electron microscopic (SEM) image of the fiber is shown in Fig. 8(a). The fiber diameter is 282 μm with 47.7 μm core size, 19.5 μm pitch size, and 2.14 μm wall thickness. The fiber cross-section is consistent with the expected surface tension influence discussed in Fig. 1. Overall, the curvature of the first two inner rings are well preserved compared to the traditional KF, hence induces smaller number of the high resonant vertices in the structure. The near field mode pattern of the 1.65 m long fabricated fiber is measured at different wavelength. Figs. 8(b) and 8(c) are the near field mode patterns at 700 nm (F = 6.42) and 1690 nm (F = 2.66) respectively. Pure fundamental-like modes can be observed at these transmission wavelengths. Fig. 8(d) plots the measured attenuation of the fabricated fiber, which is obtained by conventional cutback method with 1.65m and 0.8m fibers. The attenuation is presented in arbitrary unit because the fiber sample is too short. Nonetheless, the measured attenuation serves well in showing the distribution of the transmission windows. Red dashed lines are the calculated high resonant wavelengths (F is integer) which are consistent with the measured attenuation curve.

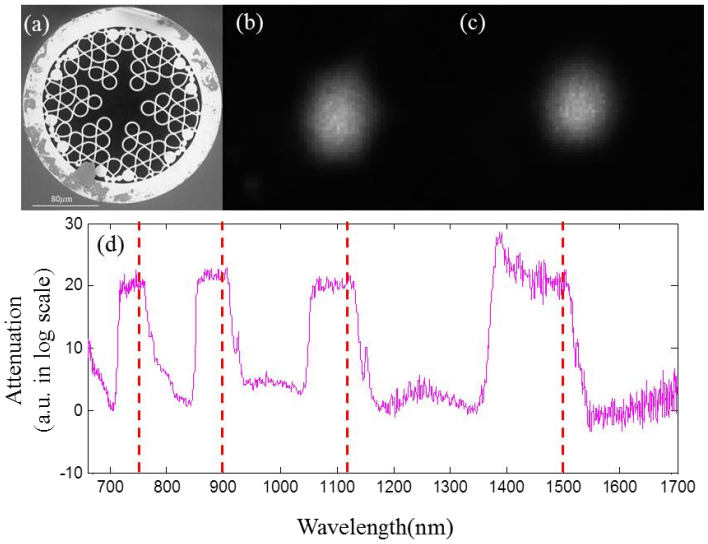

Fig. 8. (a) SEM of the fabricated 3-ring SCF. The fiber diameter is 282 μm with 47.7 μm core diameter, 19.5 μm pitch size, and 2.14 μm wall thickness. (b) Near field mode pattern at the output of 1.65 m long fabricated fiber when wavelength is 700 nm. (c) Near field mode pattern at the output of 1.65 m long fabricated fiber when wavelength is 1690 nm. (d) Measured attenuation of the fabricated fiber (deviation between the transmission of a 0.8 m fiber and a 1.65 m fiber), red dashed lines correspond to the calculated high resonant wavelengths.

4. Conclusion

In conclusion, we proposed SCFs as an alternative design for KFs. The split cladding structure is robust against fabrication deformation, and offers the below advantages:

- Low CL (comparable to CL of NANF with the same core size) due to reduced high resonant vertices and core shape deformation
- Scalable cladding layers to further reduce the transmission loss

Our simulation indicates that the SCF with two cladding layers is most efficient. The CL is substantially reduced compared to a one cladding layer structure. Such impact is more prominent in the long wavelength range. However, there is no benefit for CL from additional layers more than two.

We also found that independent control of the wall thickness and capillary size of the second ring can noticeably reduce the CL by one order of magnitude. This might suggest a new way to reduce the CL in HAFs. Moreover, the coupling between core and cladding modes is found to cause high CL. The cladding gap width also influences on the CL.

The SCF with three cladding layer was fabricated. The fabricated fiber cross-section confirms the small fabrication deformation. The measured near field mode patterns show the pure fundamental-like mode and the measured attenuation spectrum is consistent with the calculation.

Acknowledgments

The authors would like to thank Ding Wei and Wang Yingying for useful discussions. This work was supported by Singapore Ministry of Education Academic Research Fund Tier 2 (MOE2011-T2-2-120) and Agency for Science Technology and Research (A*STAR SERC 1223600002).